Conductivity deviations of constant bulk- and layer-averaged frost

T.Q. Willems[*,1], A.A. Labuschagne[1]

[*]*corresponding author t.q.willems@student.utwente.nl*
[1]*University of Twente, Faculty of Engineering Technology, Drienerlolaan 5, 7522 NB, Enschede, The Netherlands*

ABSTRACT: Air-source heat pump performance is often hindered by frost formation on the evaporator plates. Frost conductivity models aimed at mitigating the performance losses of the frost layer utilize bulk- and layer-averaged properties, ignoring differences in frost morphology. Two scripts were developed to generate frost structures and calculate their properties respectively. Air conduction above and below side branches, inter-branch interactions, and loop interactions were found to affect the total conductivity up to 3 % by analyzing aggregations of basic structures. For randomly generated samples, differences in verticality accounted for the largest conductivity differences of 5.6 %.

Key words: Frost conductivity, Effective thermal conductivity, Frost morphology, Stochastic modelling

1 INTRODUCTION

Nature contains various porous structures, of which frost is one. Frost is, amongst other locations, formed in air-source heat pumps (ASHPs) on the evaporator plates, and hinders the performance of these heat pumps due to ASHPs' interaction with air, in some stages of its growth [1]. ASHPs are installed in increasingly more households than ever before [2] and have to deal with the issues of frost growth during their operation [3], which often hinders the operational efficiency of the applications by as much as a 60% loss [1]. Heat pumps have frost-defrost cycles implemented to deal with frost formation [4], but the models used for these systems are suspected to be inaccurate, implying the unit's control system will not work as intended. This will subsequently result in more unwanted greenhouse gas emissions.

The methods currently used for modelling thermal conductivity can be divided into 3 main categories: analytical, empirical, and numerical models [5]. The first category involves models of Rayleigh, Maxwell, Maxwell-Eucken, Lewis-Nielson, Deitenberger, Le Gall et al., and many more, as well as the effective-medium theory which describes models that revolve around circular, cylindrical, or connected circular particles embedded into a matrix in a uniform or purely random dispersion [5, 6]. The second category involves experimentally determined empirical relations for the properties of a sample of microporous materials. Models such as Negrelli-Hermes, Song-Dang, O'Neal-Tree, Aurasher, and many more are often used [5, 6]. The final category entails numerical methods like FEM analysis, such as the unit cell approach proposed by Ganapathy et al. [5, 7]

The aforementioned models often use bulk or layer property simplifications to make computations or formulas more manageable [8]. However due to frost being comprised of varying structures, which produce locally varying properties [4], these simplifications introduce unwanted sporadic errors between modelled and experimental bulk properties. The exact errors are uncertain, with individual model authors measuring up to 15 % while reviewers find errors significantly more than 30 % [4, 9, 10]. This begs the question of whether different values for conductivity and diffusivity can be achieved for the same bulk and layer-averaged parameters in a frost sample and to what degree they are responsible for the deviations.

To evaluate the effect of structural influence on frost structures of uniform bulk and layer densities, frost growth as described by Hermes et al. [11], Huang et al. [12], and other authors, needs to be considered. Negrelli et al. have developed a frost-generating algorithm that can simulate both frost growth and densification [4], making it useful as a starting point for frost analysis. However, no attention was given to the structural differences, as only the bulk properties were considered. This paper will investigate the structural interactions by generating and evaluating the properties of constant bulk and layer-bulk density frost to provide more insight into the sources of the deviations measured.

2 METHODOLOGY

When modelling frost in a cell grid, a frost structure may be considered to be comprised of 3 distinct types of structures [13], see Figure 1:

1. Vertical: parallel to the heat flux direction
2. Complex: diagonal to the heat flux direction
3. Horizontal: perpendicular to heat flux direction

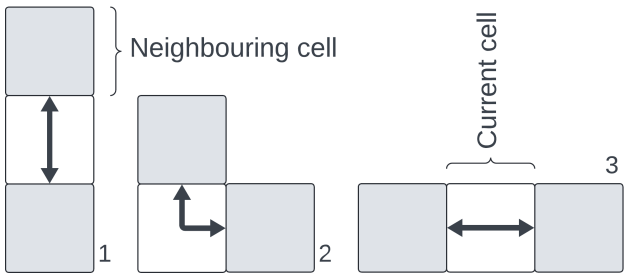

Figure 1: 1) Vertical, 2) Complex, 3) Horizontal structures. Arrows indicate the most favourable paths of conduction through the structure

To aggregate these basic structures into a singular structure, two scripts were run in MATLAB R2023a, utilizing a Windows operating system with an i7-11800H processor and 16GB of RAM. Script 1 generates aggregations of basic structures based on the input of a percentile of each type of basic structure wanted, and a predefined layer density (and thus also bulk density), as is depicted in Figure 2.

To create sufficiently varying structures, and while adhering to the density limits, permutations are used. Because the percentages from the basic structures are used to choose which location the particle aggregates to, it is likely that only the most favourable structures will be output. By allowing the algorithm to effectively choose two aggregation locations, a wider variety of structures can be analyzed. This could be increased to all locations in theory but would result in long processing times, which causes little variation in the latter stages of generation as the time-limiting loop in Figure 2 would remove most permutations.

Script 2 calculates the effective conductivity k_{eff} as

$$k_{eff} = k_{eff,cond} + k_{eff,diff} = (q''_{cond} + m'' i_{sv}) \frac{\delta}{\Delta T} \quad (1)$$

where k_{cond} and k_{diff} are the thermal conductivities considering conduction and diffusion respectively in $\frac{W}{m.K}$, q''_{cond} and m'' are the heat and diffusion fluxes across the cell border in $\frac{W}{m^2}$ and $\frac{kg}{m^2 s}$ respectively, i_{sv} is the latent heat of sublimation in $\frac{kJ}{kg}$, δ is the thickness of the cell in m, and ΔT is the temperature difference across the cell in $°C$ [14]. In this paper, Eq. (1) is decoupled to only focus on $k_{eff,cond}$ to investigate the conductivity errors introduced by structural effects without concern over errors introduced by diffusion models.

The MATLAB code as developed by Labuschagne et al. [13] is incorporated to calculate $k_{eff,cond}$ for each cell boundary, which is set at 5 μm. The values of each cell boundary are found in a 7 by 7 grid unless this size is insufficient to show all possible interactions (occurs in larger structures) or insignificant results (occurs in smaller structures). The top and bottom grid boundaries are set to $10°C$ and $0°C$ respectively. Both sides are considered to be adiabatic. The properties of ice and air are identical to those of Labuschagne et al. [13]. These calculations will be checked by MATLAB's Partial Differential Equation Toolbox version 3.10 (PDE) to verify the solutions.

The results will be analyzed in two steps. The first focuses on creating a set of similar basic structures to see what effects play a role in the conduction paths. This allows for an in-depth analysis of the behaviour of the basic types in larger structures. It is only possible to look at similar bulk density structures here and compare their conductivities with one another, seeing as the layer density is not the same for many samples. In the second step, the behavioural differences of larger samples with constant layer densities are evaluated. In addition, samples for the complete spectrum of vertical, complex and horizontal structure mixtures will be analyzed based on their thermal conductivity. Differences between the samples will be discussed using the knowledge from the first step. Lastly, the Mean Absolute Error (MAE) of the structures will be compared to that found in literature [4, 9, 10] to see how much of the observed deviations can be explained using only structural differences.

3 BASIC STRUCTURES

The basic structures are compared to one another in sets, such that the properties of each set are closely related but variations can still be made. An overview of the sets can be seen in Figure 3.

The three basic structures show trivial behaviour and will not be discussed. For combined structures, all side groups are varied in length and position, which is indicated with black arrows, to find out how con-

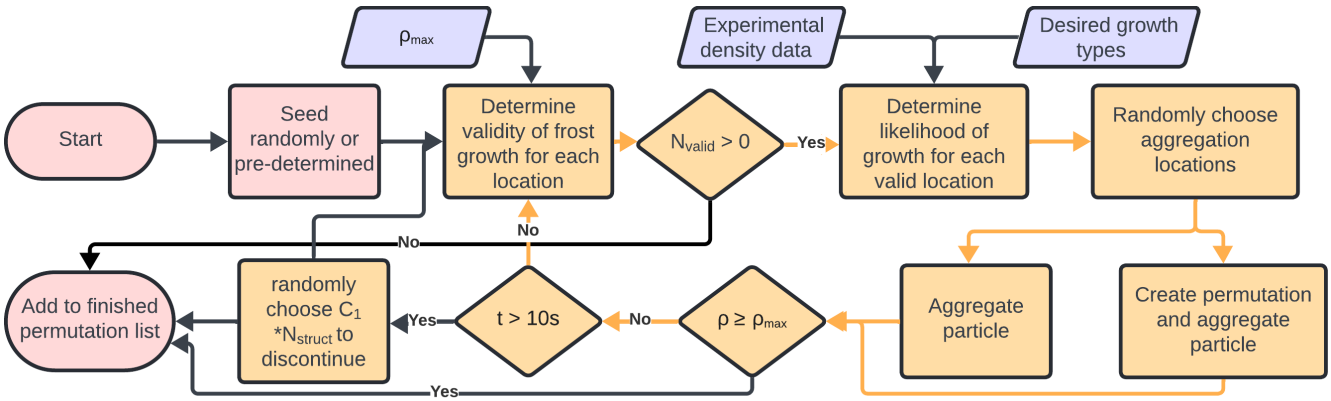

Figure 2: The frost structure generating algorithm, where the orange loop displays the main frost generation, red depicts initialization and termination, and blue shows data used. C_1 is a constant determining the percentage of structures being discontinued, N_{valid} is the number of valid growth locations, N_{struct} is the number of generated structures, ρ is the number of ice blocks present, ρ_{max} is the maximum layer or bulk density, and t is the time per orange loop for all N_{struct}.

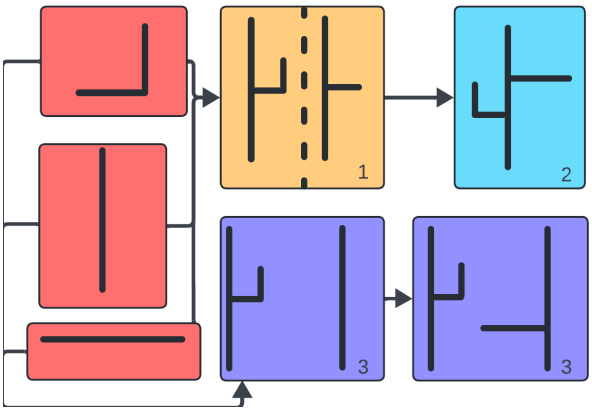

Figure 3: Compared sets, with basic structures, single vertical permutations (1 & 2), and double vertical permutations (3). Colours indicate groups with similar bulk densities

duction is influenced. Vertical growths are utilized in most structures as they will conduct most of the heat, making the findings a conservative estimate of what the side branches are capable of. Parallel and perpendicular air conduction (Q_y and Q_x respectively) one block above and below the side branches are compared. All changes in Q_y and Q_x are expressed in % and are cumulative to the initial structure. Notable conduction paths are indicated with white arrows.

It should be noted that the results from MATLAB's PDE solver were within 10% of those calculated by Script 2. A mesh with maximal edge lengths of 0.1 μm was utilized, as lower lengths resulted in changes less than 1% to the final result. The main differences between the script and the PDE solver were found in corners between blocks, which a mesh could handle more accurately than a block of 5 μm.

3.1 Set 1: single side groups

In Figure 4 a horizontal side-branch can be seen. Within the main vertical structure (MVS), almost 100

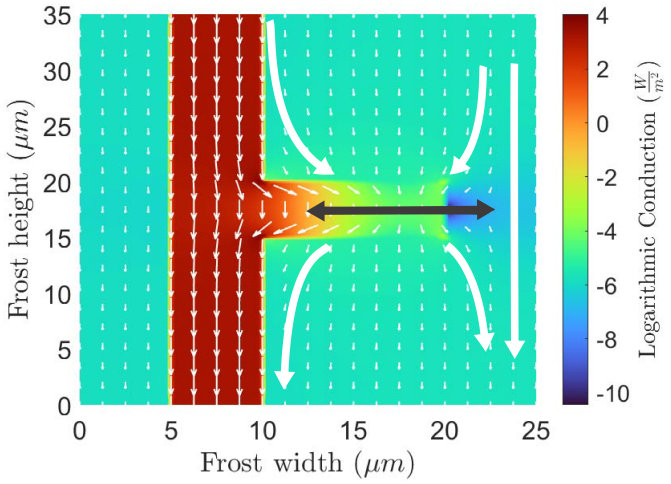

Figure 4: Structure with 2-cell wide horizontal branch showing the logarithmic conduction profile

times more heat is conducted than through the air. If even one ice block branch is present on the column, Q_y and Q_x will increase. Starting from an MVS and adding one block each time along the black arrow in Figure 4 results in an increase of Q_y by 14, 21 & 25% respectively, showing exponential decay. This implies that air layers which ordinarily would not conduct extra heat are affected by the prospect of a nearby side branch, and will conduct at most 30% extra heat, depending on the size of the side branch, which is taken from the MVS. Additionally, Q_x is in-

creased by 43% per added block compared to the previous state, meaning changes in Q_x are constant over the width of the side branch. Note that this excludes the first block being added to the MVS, seeing as this is a transition $Q_X = 0$ to some value for Q_X, which therefore would make the change approach $\infty\%$.
The exact position of the side branch only matters slightly. For edges closer to the top or bottom of the grid, no heat flux can be taken from the MVS, which means the amount of heat flux passing through the side branch decreases, making it less effective. This effect is maximally 0.4% for Q_y and 8% for Q_x, with the highest conductivity values appearing when the side branch is near the centre of the grid.
Additionally, depleted zones (in blue) are visible to the side of the side branch in Figure 4, where conduction drops to near zero due to the heat conducting into the higher conductivity side branch instead of the air, as seen by the curved white arrows on the right side. This effect is independent of branch length and always acts on the outer 2 to 3 μm.
In Figure 5 a complex side-branch can be seen, which, on the bottom, behaves similarly to a horizontal side-branch. Because the far side of the structure is

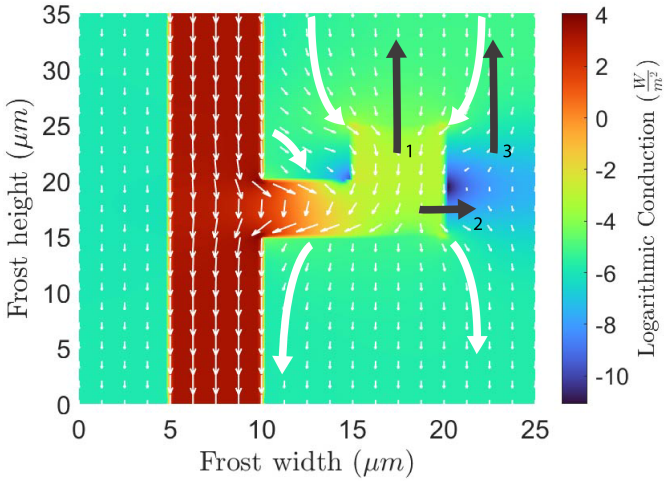

Figure 5: Structure with 2-cell wide complex branch showing the logarithmic conduction profile

two blocks tall, most heat is conducted from the MVS into the two-block tall structure, and only a small portion is conducted to the horizontal part, as depicted by the small white arrow in Figure 5.
This extra conduction in turn also introduces depleted zones. If the height of the complex structure is extended along black arrow 1, Q_Y and Q_X increase respectively with 3 & 10% and 12 & 36% compared to the case visible in Figure 5. This percentage increase is caused by the parallel vertical structure, which creates an additional route for the heat to pass through aside from the MVS. This results in a 1 & 3% increase in total conductivity of the sample for each block added respectively. If, on the other hand, the complex structure is extended along the black arrow 2, the percentage change is slightly larger than for the horizontal side branch when transitioning from two blocks wide to three blocks, namely 8 and 43% for Q_Y and Q_X respectively. However, the growth of the now extended complex side branch along black arrow 3 only results in a 2 & 5% and 7 & 20% increase for Q_Y and Q_X respectively, again showing exponential decay compared to the growth along black arrow 1. For the same bulk densities with complex side branches, the total conductivity only differs by a maximum of 3%, mainly due to the parallel vertical structure being closer to the MVS, allowing for more parallel heat transfer compared to similar bulk densities.

3.2 Set 2: mixed side groups

When two side branches are on opposite sides of an MVS, interactions occur across the MVS and between height layers, as depicted in Figure 6 by the white arrows. Here parallel conduction routes may

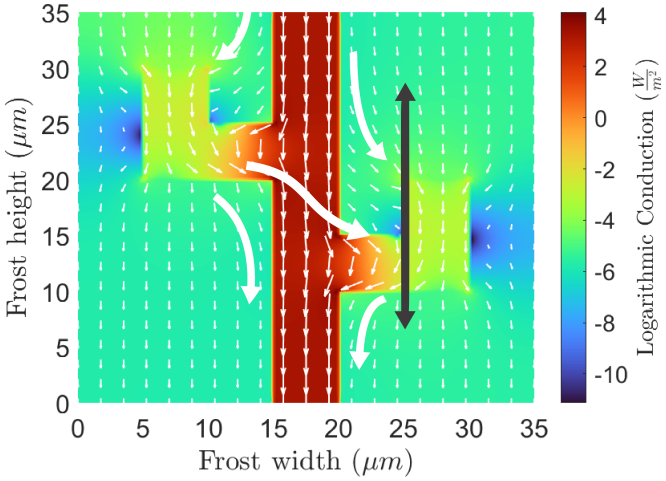

Figure 6: Structure with two opposing complex branches showing the logarithmic conduction profile

be created depending on the position of the side branches. The route becomes less parallel whenever the side branches move further away from one another, as seen in the changes in Q_x, which changes 5, 7 & 9% along the black arrow from an initial symmetric case. This indicates that heat is initially

transported purely symmetrically, then both a parallel route and sequential routes are used, and lastly, purely sequential heat travel is utilized once the structures are further than 15 μm apart from one another. This sequential route mimics the behaviour of the complex branch growing along black arrow 1 in Figure 5. Once the heat from the left complex branch can reach the lower branch's top part, heat can move into the MVS and to the next parallel path, increasing the total conductivity. Q_y changes 0.3, 0.6 & 3% along the black arrow from an initial symmetric case, meaning if the position of the complex branch is 5 μm lower than in Figure 6, the sequential route is used. If both branches are on the same side, the sequential route is always utilized, but heat is still exchanged with the MVS if the branches are sufficiently far apart. For either branch orientation, the average conductivity changes less than 0.5% due to the absence of major parallel routes

A connecting structure can be formed in a multitude of ways, of which Figure 7 is one example.

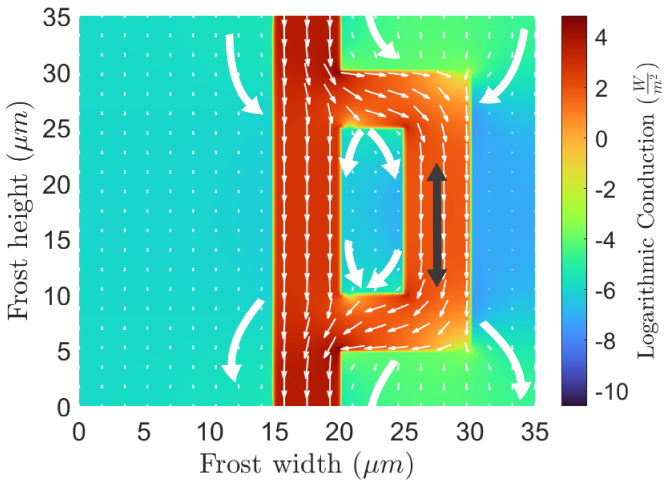

Figure 7: Structure with connected complex and horizontal branch showing the logarithmic conduction profile

When side branches grow into one another, they can create a loop. This loop is a favourable path and conduction through the branch increases by roughly 7% if the loop length is increased by one block along the black arrow. Additionally, Q_y above and below the loop indicated with white arrows increases 10, 21 & 49% compared to the smallest loop possible. This relates back to the creation of parallel paths, but the effect is stronger than in set 1, seeing as the path connects back to the MVS. This finding is enforced by looking at the magnitude of conduction within the loop branch versus the MVS. Taking the conduction in the MVS as 100%, the side branch conducts 36, 49, 53 & 59% of that for each length increase of the loop. The air trapped inside the loop shows a split between two different effects. Near the MVS, similar behaviour to a horizontal side branch is observed, namely heat is taken from and added back to the MVS before and after the branch respectively, while further to the right the heat is redirected into the loop, contributing to the conduction increase in the parallel route.

The conduction in the depleted zone past 30 μm in Figure 7 is a factor 10 larger than that of a single side branch (0.02 and 0.002 $\frac{W}{m^2}$ respectively). This conductance field is more parallel-oriented than a single side branch, as all the heat that wants to conduct into the side branch has already done so at the top and bottom, leaving only "stray heat" to conduct through the air, which is almost two times less than the heat on the left side of the MVS, this being 0.035 $\frac{W}{m^2}$.

3.3 Set 3: double vertical with single side groups

When two MVSs are present, interactions between side branches between the two columns also occur. This can be seen in Figure 8, where a complex side branch provides a connection between the two columns. When the lower branch extends along black

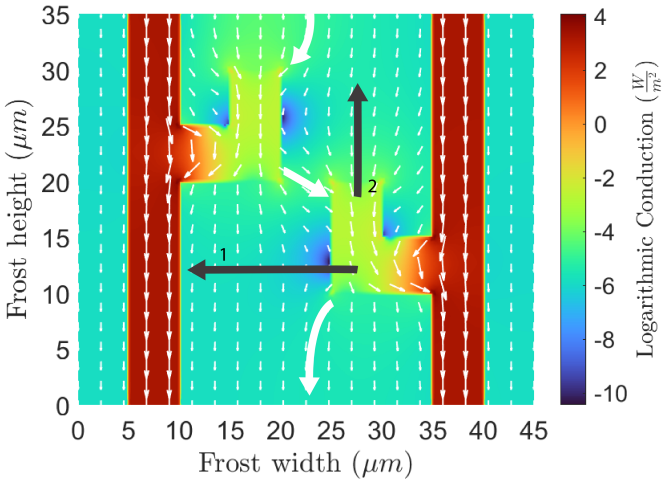

Figure 8: Structure with two opposing complex branches showing the logarithmic conduction profile

arrow 1, the average conductivity only changes significantly (2%) when the branch connects to the other MVS. This connection also causes a decrease in Q_y, as heat exchanging between MVSs is now preferred over air conduction. Growth along black arrow 2 of more than 10 μm creates a parallel route but alters the

conduction path between the two complex branches. Instead of the conduction from the left MVS towards the right MVS occurring in a rough diagonal line, most conduction would follow the grown complex branch and thus require much more Q_x to use this parallel route effectively. This can hinder Q_y by as much as 3%. For the heat that does not take this diagonal route, a parallel route is instead formed along the white arrows in Figure 8, which has the same restrictions regarding the position of the side branches as set 2.

3.4 Comparison between different sets

Taking a step back from the inner workings of each structure and comparing the overall conductivities to existing models [5, 15] as suggested by Labuschagne at al. [13], Figure 9 can be made.

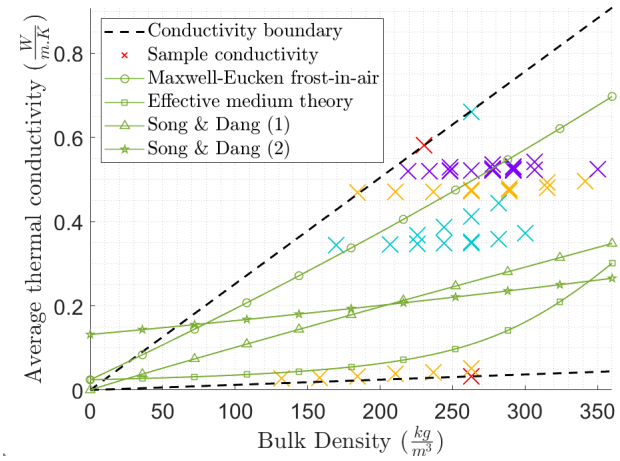

Figure 9: Comparison of the set structures' thermal conductivity versus bulk density. Colours show different sample sets as depicted in Figure 3. Existing heterogeneous material models from Maxwell-Euken [5], Effective medium theory [5] and the work of Song and Dang [15] are included for reference

As evident from the previously described sets, the variations among different structures are quite minimal, but by comparing similar bulk densities, the observed variations are quite significant. For example, the blue samples indicate structures in set 2, where simple side branches (low density) like purely complex and horizontal are near the upper conductivity limit, and more grown-out structures are further and more dispersed from this limit, accentuating the structural interactions between different structures and this deviation will be investigated further.
Comparing the samples to existing theories for thermal conductivity in frost, such as models by Song and Dang [15], indicates non-conformity with real frost, as the MAE is upwards of 75%. This suggests that these models are not fit for predicting these basic structures, implying the structures that will be generated in the next chapter should take the typical growth characteristics of frost into account to be a valid comparison.

4 ARBITRARY STRUCTURES

4.1 Model validation

By arbitrarily generating structures using Script 1, a spectrum of different structures can be found. Figure 10 was made by assigning the same input parameters and running the script multiple times to validate Script 1. A maximum standard deviation σ of

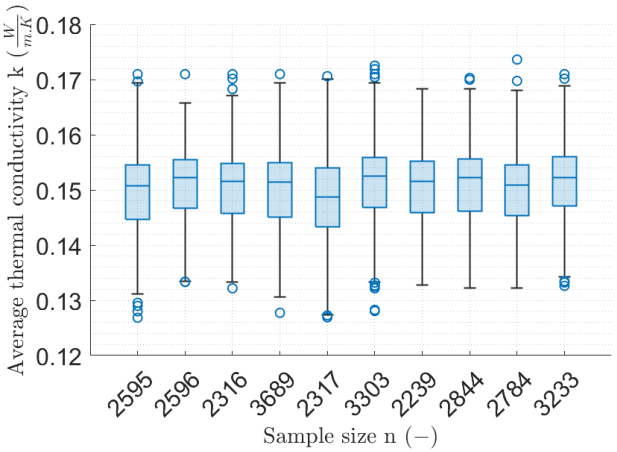

Figure 10: Comparison of 10 samples generated by Script 1 with the same input parameters and a bulk density of 375.4 $\frac{kg}{m^3}$

0.0015 and a maximum difference in averages μ of 0.001 was found, which, using Operating Characteristic Curves [16], results in a needed sample size of at least 20 samples for each possible combination of vertical, horizontal, and complex structures to reach a 95% confidence interval, with a type II error rate of 10%. Additionally, a maximum MAE of 5.4% is found throughout all script checks, accounting for the modelling error that might occur when using a sampling approach like Script 1.

4.2 Conductivity spectrum

Structures with the same initial seeding location, bulk density, and layer density, spanning the entire spectrum unit mixture requirements were used to find values for the average thermal conductivity of frost. This

can be seen in Figure 11. A clear gradient can be

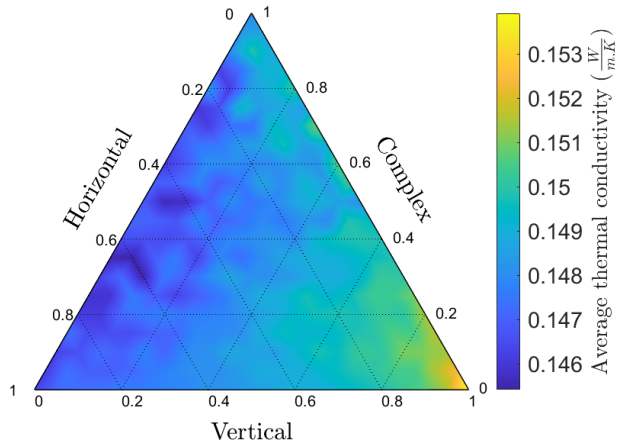

Figure 11: Average thermal conductivity of 20 samples versus input unit mixture requirement, with a layer density of 393.7 $\frac{kg}{m^3}$

seen, with vertical structures being the main determinator of conductivity. As was already seen in the analyzed sets, the more vertical a structure grows, the more conductive it becomes. Change in the percentage of vertical structures can account for 5.6% of the conductivity deviation for the same layer density. A low likelihood of horizontal growth can increase the conductivity by roughly 2%, suggesting branch interactivity plays a role between more grown-out branches. However, this spectrum only specifies the input settings. The same results over the output unit mixtures are depicted in Figure 12.

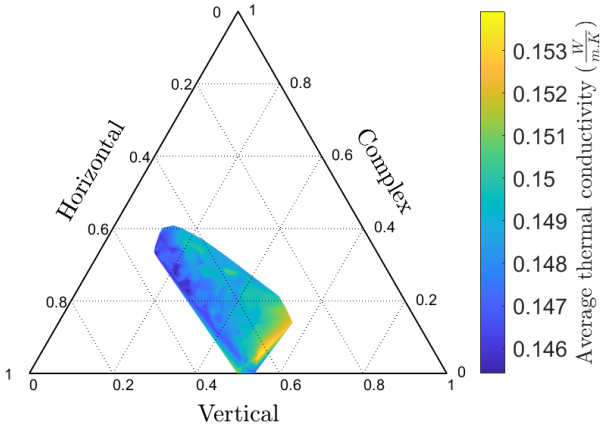

Figure 12: Average thermal conductivity of 20 samples versus successfully generated output unit mixtures, with a layer density of 393.7 $\frac{kg}{m^3}$

Even though the same data points are used, the actual domain spans only a fraction of what is possible. In this case, the domain is limited by the need for vertical growth as the layer density needs to be reached. At least one vertical or complex block is necessary to reach the next layer, resulting in a lack of data in the bottom left corner. Therefore, most data points, especially the low % vertical mixtures, are visible on the 66% line of horizontal growth. The 7 by 7 grid used for all samples currently limits the onward growth of vertical and complex structures. Different grid sizes and an increased number of nucleation locations may be able to generate more sample points in currently unknown areas. The standard deviation of the samples versus input unit mixture settings can be seen in Figure 13 and is much higher at higher complex growth.

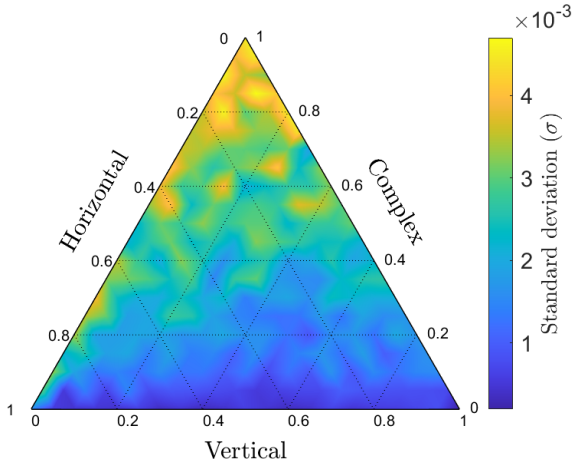

Figure 13: Average standard deviation of 20 thermal conductivity samples versus input unit mixture requirement, with a layer density of 393.7 $\frac{kg}{m^3}$

A couple of reasons arise for this difference, with the main reason being the sample size. Low complex-containing structures generate datasets which are a factor of 10 larger than those with more complex branches, due to how complex branches are generated. If a location is chosen to be complex growth, the two subsequent growth locations will necessarily be the two cells needed to 'complete' the complex structure, thus not generating permutations. An influence of verticality can also be seen in Figure 13, where extremely low verticality causes larger deviations in conductivity. This is most likely because of the many side-branches, between which interactions can occur. The orientation of these branches matters in this region, as 1 block difference would cause Q_y to be much more impactful on the overall conductivity due to branch interactions as mentioned in Section 3. Using this (somewhat limited) dataset, a possible 11,0% of the 15,0 to 31,9% MAE found in literature [9, 10] can be accounted for by structural influences.

5 CONCLUSION

An analysis of possible structural causes for deviations in thermal conductivity was performed by first evaluating simple structures with basic side branches to understand the conduction behaviour in frost crystals. Local conductivity increases were observed due to the branch interactions with air. Interactions amongst sufficiently nearby side branches were also observed, which may contribute to experimental deviations. Comparing sets based on bulk density in Figure 9 showed clear deviations in thermal conductivity. Even comparing the same layer densities, deviations were observed, however smaller at a maximum of 5.6%. The full spectrum of output structures could not be found due to model limitations, as shown in Figure 12. Deviations are expected to increase when the full spectrum is modelled, which may be achieved by additional seeding locations, expanding the growth domain, different initial seeding locations, and varying layer densities. In the current work, a possible 11,0% of the 15,0 to 31,9% MAE found in literature [9, 10] could be explained.

ACKNOWLEDGEMENTS

The corresponding author would like to thank Tim van den Berg for his experimental data on frost densities, which was used to obtain more accurate generated structures.

AVAILABILITY OF DATA AND MATERIALS

Supplementary materials are available upon request from t.q.willems@student.utwente.nl.

REFERENCES

"During the preparation of this work the author(s) used no artificial intelligence tools."

[1] Y. Li, M. Li, Y. Utaka, T. Daitoku, H. Ohkubo, and C. Yang, "Scraping force characteristics of frost formed on vertical cooling surfaces having different structures and wettability," *International Journal of Refrigeration*, vol. 101, pp. 148–154, 2019. doi:10.1016/j.ijrefrig.2019.03.014.

[2] IEA, "The future of heat pumps," *World Energy Outlook Special Report; International Energy Agency, Paris, France*, 2022. doi:10.1787/2bd71107-en.

[3] M. Kandula, "Effective thermal conductivity of frost considering mass diffusion and eddy convection," *Special Topics & Reviews in Porous Media: An International Journal*, vol. 1, no. 4, 2010. doi:10.1615/SpecialTopicsRevPorousMedia.v1.i4.40.

[4] S. Negrelli, R. P. Cardoso, and C. J. Hermes, "A finite-volume diffusion-limited aggregation model for predicting the effective thermal conductivity of frost," *International Journal of Heat and Mass Transfer*, vol. 101, pp. 1263–1272, 2016. doi:10.1016/j.ijheatmasstransfer.2016.05.135.

[5] K. Pietrak and T. S. Wiśniewski, "A review of models for effective thermal conductivity of composite materials.," *Journal of Power Technologies*, vol. 95, no. 1, 2015. ISSN:2083-4195.

[6] J. Shin, A. V. Tikhonov, and C. Kim, "Experimental study on frost structure on surfaces with different hydrophilicity: density and thermal conductivity," *J. Heat Transfer*, vol. 125, no. 1, pp. 84–94, 2003. doi:10.1115/1.1518496.

[7] D. Ganapathy, K. Singh, P. E. Phelan, and R. Prasher, "An effective unit cell approach to compute the thermal conductivity of composites with cylindrical particles," *Journal of Heat Transfer*, vol. 127, no. 6, pp. 553–59, 2005. doi:10.1115/1.1915387.

[8] J. Al-Ghalith, T. Dumitrică, J. Al-Ghalith, and T. Dumitrica, "Deformed carbon nanotubes," *Nano-scale Heat Transfer in Nanostructures: Toward Understanding and Engineering Thermal Transport*, pp. 55–78, 2018. ISBN:9783319738819.

[9] A. Leoni, M. Mondot, F. Durier, R. Revellin, and P. Haberschill, "Frost formation and development on flat plate: Experimental investigation and comparison to predictive methods," *Experimental Thermal and Fluid Science*, vol. 88, pp. 220–233, 2017. doi:10.1016/j.expthermflusci.2017.06.005.

[10] S. Negrelli, V. S. Nascimento Jr, and C. J. Hermes, "A study of the effective thermal conductivity of frost formed on parallel plate channels," *Experimental Thermal and Fluid Science*, vol. 78, pp. 301–308, 2016. doi:10.1016/j.expthermflusci.2016.06.019.

[11] C. J. Hermes, J. Boeng, D. L. da Silva, F. T. Knabben, and A. D. Sommers, "Evaporator frosting in refrigerating appliances: Fundamentals and applications," *Energies*, vol. 14, no. 18, p. 5991, 2021. doi:10.3390/en14185991.

[12] C. Huang, Y. Zhao, and T. Gu, "Ice dendrite growth atop a frozen drop under natural convection conditions," *Crystals*, vol. 12, no. 3, p. 323, 2022. doi:10.3390/cryst12030323.

[13] A. Labuschagne, T. Zhu, and W. Rohlfs, "Micro-ct investigation of urea crystal structures for frost analysis." University of Twente: Department of Thermal and Fluid Engineering, Faculty of Engineering Technology (ET), unpublished, 2024.

[14] H. Auracher, "Effective thermal conductivity of frost," in *International Symposium on Heat and Mass Transfer in Refrigeration and Cryogenics*, Begel House Inc., 1986. doi:10.1615/ICHMT.1986.IntSympHMTinRefCryo.

[15] M. Song and C. Dang, "Review on the measurement and calculation of frost characteristics," *International Journal of Heat and Mass Transfer*, vol. 124, pp. 586–614, 2018. doi:10.1016/j.ijheatmasstransfer.2018.03.094.

[16] D. C. Montgomery and G. C. Runger, *Applied statistics and probability for engineers*. John wiley & sons, 2010. ISBN:978-1-119-40030-1.